JOURNAL OF NANO- AND ELECTRONIC PHYSICS
Vol. **5** No 4, 04059(5pp) (2013)

ЖУРНАЛ НАНО- ТА ЕЛЕКТРОННОЇ ФІЗИКИ
Том **5** № 4, 04059(5cc) (2013)

Investigating Impact of The Interfacial Debonding on The Mechanical Properties of NanoFiber Reinforced Composites

Waleed.K. Ahmed*

United Arab Emirates University, Faculty of Engineering, ERU, Al Ain 15551 UAE

(Received 12 July 2013; published online 31 January 2014)

This work investigates the influence of the interfacial debonding in a nanofiber reinforced composite on the mechanical properties. Mainly, three dimensional-axisymmetric finite element analysis is adopted to study a representative volume element (RVE) which is consist of carbon nanofiber confined by a polymeric matrix and subjected to axial tension. Besides, a longitudinal interfacial debonding is imposed along the interfacial nanofiber/matrix. The result of the FEA demonstrate a significant impact of the interfacial debonding on the Young's modulus of the nanocomposite.

Keywords: Composite, Debonding, FEA, Interfacial, Mechanical properties, Nanofiber.

PACS numbers: 02.70. – c, 46.50. + a, 81.05.Qk

1. INTRODUCTION

Nanocomposites are a novel class of composite materials where one of the constituents has dimensions in the range 1-100 nm [1]. They can be produced by embedding reinforcement in the form of nanofibres or nanotubes in a matrix such as a polymer in a similar manner to conventional composite materials [2]. Nanocomposites is considered as one of the growing areas of nanotechnology, since CNTs have remarkable mechanical properties and is intensively used as reinforcements in polymers and other matrices to form what is nowadays is called "Nanocomposite materials"[3]. Nanofibers in general, and the nanotubes in particular, can be hundred times stronger than steel and even more than six times lighter, become as a candidate for aerospace application [4]. Moreover, nanotubes show increasing in composite strength by as much as 25 % [5]. Nanocomposites' reinforcement can include nanofibers, nanoplatelets and nanoclay. These reinforcements are functionalized with additives, by this means resulting in a strong interfacial bond with the matrix [1]. Mainly, there are three mechanisms of interfacial load transfer between nanofiber and the matrix, which are the weak van der Waals force and the reinforcement, chemical bonding, and micromechanical interlocking [6]. Mainly, there are two causes behind a mechanically strong or weak nanocomposite material which affects the stiffness, the matrix interface with the nanofibers and the stress transfer. As the nanocomposite subjected to mechanical loading, stress concentrations will take place at the matrix/nanofiber interface which will eventually lead weakness of the nanocomposite and eventually lead to damage nucleation, initiation, growth and final non-tolerated failure [7]. There are two probable sources of damage nucleation in nanocomposites; poor wetting of the nanofibers by the polymer and the aggregation of the nanofibers [8]. Both cases produce polymer rich nanocomposite portions that are likely to experience low stress to failure. Researchers [9] have observed that one of the reasons that nanocomposites may have a low strain to failure is the high interfacial stress that can lead to nanofiber / matrix debonding. In addition, the stress transfer from the matrix to the reinforcement is the main factor that will dictate the final nanocomposite material strength. It is reported that load transfer through a shear stress mechanism was observed at the molecular level [1]. Moreover, local interfacial properties affect the macrolevel material behavior, like reduction in flexural strength in nanotube / epoxy composite beams due to weakly bonded interfaces [10], as well the reduction in composite stiffness which was attributed to local nanofibers/ nanotube waviness [11], whereas the impact of the interfacial crack [12], mismatch [13] and the nanoinclusion [14] on the interfacial stresses in nanocomposite were investigated using finite element method. As a results, deterioration of the nanocomposite's mechanical properties can be attributed to many factors, therefore it has been attracted many researches to investigate the effective Young's modulus as well as the parameters that play big role in the predicted properties. Gawandi et al [15] investigated the influence of the nanofiber elastic properties and toughening effect of the nanofiber by 3D-FE of a penny-shaped cracked matrix as well as the impact of mismatch. Whereas a representative volume element (RVE) of a simplified 3D model for a wavy carbon nanotube (CNT) is considered [16] to study the stress transfer in (SWCNT) composites. The adopted model was capable of predicting axial as well as interfacial shear stresses along a wavy CNT embedded in a matrix. Moreover, the effects of the waviness of the CNTs and the interfacial debonding between them and the matrix on the effective moduli of CNT–reinforced composites are studied by a simple analytical model to investigate the influence of the waviness and debonding on the effective moduli [17]. A computational numerical-analytical model of nano-reinforced polymer composites is developed taking into account the interface and particle clustering effects [18]. The model was employed to analyze the interrelationships between microstructures and mechanical properties of nanocomposites. An improved effective interface model which is based on Mori-Tanaka approach and includes the nanoparticle geometry and clustering ef-

* W.ahmed@uaeu.ac.ae

fects was developed. Yijun et al used advanced boundary element method (BEM) to study curved cracks at the interphases between the fiber and matrix in the fiber reinforced composites, where stress intensity factors (SIFs) are evaluated and the interface cracks at the interphases of fiber-reinforced composites are studied and the effects of the thickness and materials on the SIFs are investigated. The effects of spatial distribution and geometry of carbon nanotubes (CNTs) on the macroscopic stiffness and microscopic stresses of CNT reinforced polymer composites are investigated based on the multi-scale homogenization theory [20], besides the influence of the aspect ratio and volume fraction of CNT, the end gap between two coaxial nanotubes and the distance between two parallel nanotubes on the nanocomposites are also investigated. An extensive review of the work done of experiment, theory of micro-nanomechanics, and numerical analysis on characterizing mechanical properties of nanocomposites is presented [21]. Three different approaches are discussed in finite element modeling, i.e. multiscale representative volume element (RVE) modeling, unit cell modeling, and object-oriented modeling. Also, the mechanism of nanocomposite mechanical property enhancement and the ways to improve stiffness and fracture toughness for nanocomposites are discussed. Unnati et al [22] studied the effects of pinhole defects on the mechanical properties are investigated for wavy carbon nanotubes based nanocomposites using 3D RVE with long carbon nanotubes. The Young's modulus of elasticity are evaluated for various values of waviness index, as well as type and number of pinhole defects under an axial loading condition. The presence of chemical bonding between functionalized carbon nanotubes and matrix in carbon nanotube reinforced composites is modeled by elastic beam elements representing covalent bonding characteristics by neglecting reinforcing mechanisms in the composite such as relatively weak interatomic Van der Waals forces [23]. The effective mechanical properties of CNT-based composites are evaluated using a square RVE based on the continuum mechanics and with FEM [24]. Besides, formulas to extract the effective material constants from solutions for the square RVEs under two load cases are derived based on the elasticity theory. Rafiee et al [25] investigated the impact of CNTs on the fracture behaviour by estimating J-integral of composites using A 3D FEM consisting of CNT, interphase and surrounding polymer is constructed. CNT is modeled as a lattice structure using beam elements and the interphase region is simulated using non-bonded interactions. The longitudinal behavior of a CNT in a polymeric matrix is studied [26] using a non-linear analysis of a full 3D multi-scale FEM consisting of carbon nanotube, non-bonded interphase region and surrounding polymer. The bonding between carbon nanotube and its surrounding polymer is treated as van der Waals interactions and corresponding longitudinal, transverse and shear moduli are calculated. Based on molecular mechanics, an improved 3D-FEM for armchair, zigzag and chiral single-walled carbon nanotubes (SWNTs) was developed [27] and the bending stiffness of the graphene layer was considered. The elastic stiffness of graphene was studied and the effects of diameters and helicity on Young's modulus and the shear modulus of SWNTs were investigated. Tserpes and Chanteli evaluated the effective elastic properties of carbon nanotube-reinforced polymers as functions of material and geometrical parameters using a homogenized RVE and 3D FE model. The parameters considered are the nanotube aspect ratio, the nanotube volume fraction as well as the interface stiffness and thickness. Both isotropic and orthotropic material properties have been considered for the MWCNT. Atomistic-based FE analysis is combined with mechanics of materials to evaluate the geometrical characteristics and elastic properties of beams by using 3D FE analysis and a linear behavior of the C-C bonds to estimate the tensile, bending and torsional rigidities of CNTs [29]. A developed FEM based on molecular mechanics to predict the ultimate strength and strain of SWCNT, and the interactions between atoms was modeled by combining the use of non-linear elastic and torsional elastic spring. Mechanical properties as Young's modulus, ultimate strength and strain for several CNTs were calculated [30]. Hernández-Pérez and Avilés [31] investigated the influence of the interphase on the effective properties CNT composites using FEA and elasticity solutions for RVEs and the influence of the thickness and gradient in elastic modulus on the elastic properties and stress distribution of the composite is examined. A proposed SWCNT-FEM, based on the use of nonlinear and torsional spring elements is adopted [32] to evaluate the mechanical properties. The influence of tube diameter and chirality on the Young's modulus of SWCNTs was investigated, armchair, zig-zag and chiral nanotubes, with different size, were tested under uniaxial load.

The present paper investigates through using the finite element analysis the significances of the debonding between the nanofiber and the matrix of nanocomposite. Mainly, the proposed debonding is modeled to be existing between the nanofiber and the matrix as a longitudinal defected zone. Therefore, the impact of this debonding will be studied and discussed in term of the stiffness of the representative volume element (RVE), i.e., effective Young's modulus. Linear elastic analysis is chosen as the basis for the present analysis using finite element analysis. Uniaxial load is imposed to study the case, whereas three different values of the reinforcements' stiffness are used to model the nanofibers' properties. Each case are investigated individually through using traditional package ANSYS to predict normal and shear stresses along the interfacial nanofiber/matrix for both debonded and intact RVE. Representative volume element (RVE) was proposed to model the case, and 3D-axisymmetric dimensional analyses are implemented to model the nanocomposite because of the complexity of the problem.

2. FINITE ELEMENT ANALYSIS

Finite element analysis (FEA) has been used by researchers as a powerful tool in investigating the interfacial stresses, the failure strains as well as the effective Young's modulus of the nanocomposites instead of molecular dynamic simulation [6], since the latter can only deal with physical phenomena at the level of a few nanometers at the present stage, whereas the size of a representative volume of a nanocomposite material ranges from 10 nm upward to several hundreds of nanometers.

It was reported that mostly the smallest dimension of the nanofiber under investigation of the researchers lies in the range 20-50 nm, therefore continuum mechanics assumptions, like the one used in the finite element analysis are still valid at such length scales. Analogous finite element analyses have been reported by [16] with a focus on stiffness analysis incorporating micromechanics theory. In fact, these finite element analyses simplified the complex interaction among the nanoscale reinforcement, matrix and the doable interphase [6].

In this paper, the aim of the finite element analysis (FEA) is to investigate the impact of a proposed debonding between the matrix and the reinforcement, i.e., nanofiber, on the effective Young's modulus of the nanocomposite. Moreover, the analysis explores the interfacial normal and shear stresses along the nanofiber sides. The FEA modeling was carried out using ANSYS software. In order to simplify the modeling of the study, 3D-axisymmetric dimension analyses were conducted by FEA which is mainly based on a cylindrical representative volume element (RVE) of the nanocomposite material. Besides, constituents properties of the nanoreinforcement and the matrix have been obtained used similar to the previous investigators [6]. The proposed RVE model as well as the interfacial debonding used in this study is shown in Fig. 1, whereas Fig. 2 illustrates the 3D axisymmetric FE model and the boundary conditions used in the analysis.

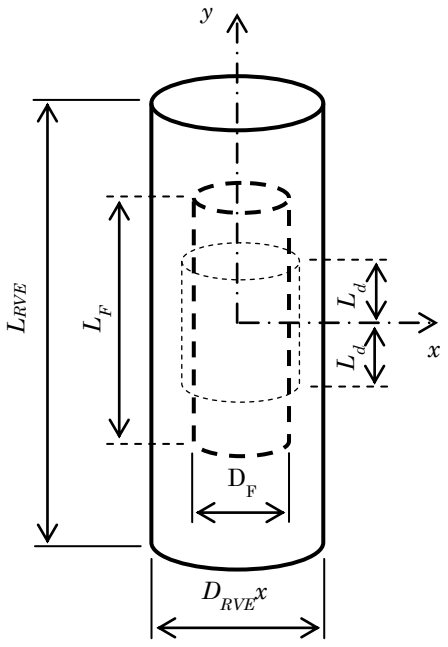

Fig. 1 – Cylindrical RVE reinforced by nanofiber with circumferential interfacial debonding

Due to complexity of the problem, 3D-axiymmertic finite element analysis is carried out to model the nanofiber composite, i.e., RVE. Four-node quadrilateral element (solid 182) is employed in the investigation through ANSYS software to assess the effective stiffness, i.e., Young's modulus, as well as the interfacial stresses along the nanofiber. The interfacial debonding is modeled as circumferential sharp crack. Tie constraints are applied locally at the interface between the

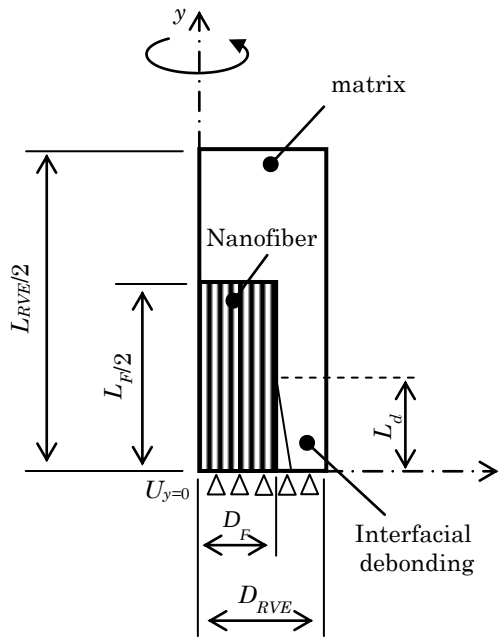

Fig. 2 – 3D-Axisymmetric FE model with boundary conditions

nanofiber and the matrix except for the debonding line L_d in order to represent the interfacial debonding zone. A dense mesh in and around the nanofiber-matrix interface to a relatively coarser mesh utilized for the rest of the RVE.

3. GEOMETRY AND MATERIALS SPECIFICATION

The material properties used in the baseline RVE is epoxy matrix has a Young's modulus of $E_m = 4$ GPa and Poisson's ration of $\nu_m = 0.4$. Analogous to other finite element analyses done previously [6], the nanofiber is considered as transversely isotropic materials [14]. The nanofiber is considered as a carbon fiber of elastic modulus of $E_f = 200$, 400 and 1000 GPa respectively. A tensile stress of unit nN / nm^2 is applied on the nanocomposite and imposed to be parallel to the longitudinal nanofiber of the nanocomposite, whereas the transvers direction of the nanocomposite is left free of any load.

The adopted cylindrical RVE of the proposed nanocomposite is proposed to have a length of $L_{RVE} = 120$ nm and diameter of $D_{RVE} = 90$ nm. The RVE consist of a matrix of polymer and a nanofiber. The nanofiber has a cylindrical shape of $L_f = 100$ nm and $D_f = 20$ nm which is equivalent to $L_{RVE} / L_f = 1.2$ and $D_{RVE} / D_f = 4.5$ which can be expressed by a fiber volume fraction of the nanocomposite $V_f = 4$ %.

The debonding length along the longitudinal side of the nanofiber L_d of 0, 10, 25, 40 and 50 nm is considered in the analysis for the cases studied, and this value is corresponded to debonding length to the nanofiber's length of $L_d / L_f = 0$, 0.2, 0.5, 0.8 and 1, where intact RVE whenever $L_d / L_f = 0$ which si the standard case, whereas the fully debonding case when $L_d / L_f = 1$. The nanofiber and the matrix in the model are assumed to be bonded perfectly with the exception of the debonding line. Frictionless sliding behavior is assumed between the mismatch's faces.

The level of the local interfacial stresses arises at the debonding line are inspected as well. The defected nanocomposite, i.e., debonded, is investigated under static loading conditions for uniaxial tensile stress. In addition, the debonding length L_d along the longitudinal side of the nanofiber is considered as parameters in the analysis through the analysis. Nanofiber's stiffness is considered as another parameter in the analysis.

The impact of the longitudinal debonding on the longitudinal side of the nanofiber is studied to estimate the effective Young's modulus and for both interfacial normal stresses σ_y along the nanofiber's diameter and the shear stresses τ_{xy} as well as Von Misses stresses along the nanofiber's side. It is important to mention that effective Young's modulus of the nanpocomposite is estimated through longitudinal displacement results by imposing multipoint constraints (MPC) on the cylindrical RVE along RVE's diameter.

4. RESULTS AND DISCUSSION

In the FE analysis of the RVE which contains longitudinal debonding, the impact of the debonding to the nanofiber length $2L_d / L_f$ on the effective Young's as well as the interfacial normal, shear and Von Misses stresses and are investigated in three stages.

In stage I, the effective Young's modulus of the RVE is investigated due to presumed debonding, whereas in stage two the normal and Von Misses stresses along the transverse side of the nanofiber is investigated, whereas in the last stage, the longitudinal shear and Von Mises stresses are estimated. The main parameters in the analysis are the debonding length ratio, i.e., $2L_d / L_f$ which has value of 0, 0.2, 0.5, 0.8 and 1 respectively, whereas the nanofiber's stiffness values are $E_f / E_m = 50$, 100 and 250.

It is observed from Fig. 3 increases in the effective Young's modulus of the intact RVE to be 1.54 times the matrix stiffness for the $E_f / E_m = 50$ case, whereas rises from 1.64 to 1.71 as the E_f / E_m varies from 100 to 250, this attributed to the impact of the reinforcement's stiffness. As the debonding introduces, a significant reduction in the normalized effective Young's modulus of 1.3 % when $L_d = 10$ nm, where it is observed to b almost constant between $2L_d / L_f = 0.2$ to 0.5. After crossing $2L_d / L_f = 0.6$, the second stage reduction in normalized effective Young's modulus occur up to total reduction in stiffness of 6.5 % for the $E_f = 200$ GPa whereas this maximum value becomes 7.4 % and 9.4 % for both $E_f = 400$ and 1000 GPa respectively as the RVE becomes fully debonded in the longitudinal direction. That means, as the debonding increases, the impact of the nanofiber's stiffness becomes negative on the effective Young's modulus.

Normal stress σ_y and Von Misses stresses von are estimated along the transverse side of the nanofibers as the debonding progresses through the longitudinal side of the nanofiber. Figure 4 illustrates a drop in normalized σ_y up to 10.7 % as debonding approaches 10 nm, whereas almost remains constant through the progress of the debonding from $L_d = 10$ to 80 nm. Beyond this limit, a significant rise in normalized σ_y observed to be 62.5 % as RVE becomes fully debonded, and this attributed to the stresses at the transvers side started to carry the whole applied stresses, and this may cause peeling failure between nanofiber and the matrix. This is for $E_f / E_m = 50$, for the other stiffness ratio, the maximum normalized stress approaches 61.9 and 62.3 % for the $E_f = 400$ and 1000 GPa respectively.

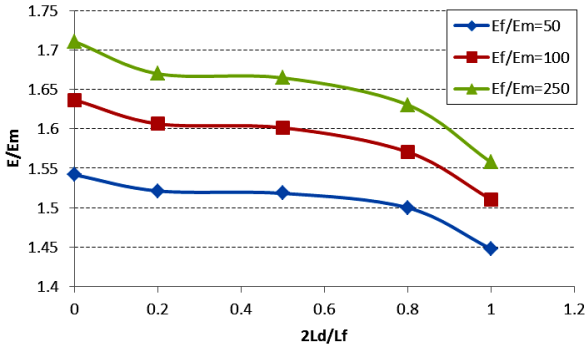

Fig. 3 – Normalized effective Young's modulus E / Em versus total debonding length over nanofiber's length

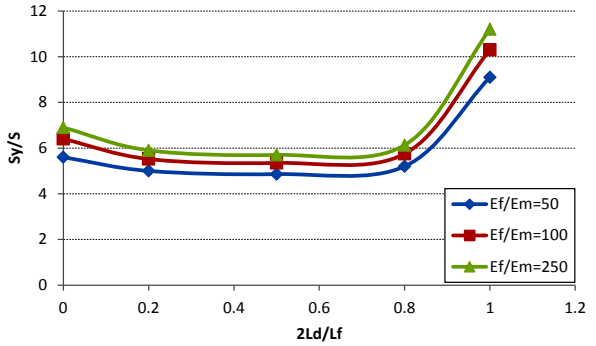

Fig. 4 – Normalized stress of transverse side σ_y/σ versus total debonding length over nanofiber's length

In the other hand, the Von Misses stresses along the transverse side shows a quit similar behavior but a little bit higher stresses, as shown in Fig. 5, and this is expected due to combined load effect. As in the normal stresses σ_y, there is a drop in stresses about 15.7 % at $L_d = 10$ nm and remains almost steady up to $L_d = 80$ nm.

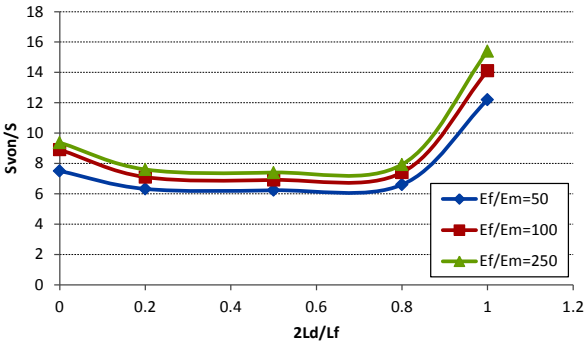

Fig. 5 – Normalized Von Misses stress of transverse side σ_{Von} / σ versus total debonding length over nanofiber's length

After that an increase in stresses up to 62.6 % as RVE becomes fully debonded, and this value exactly the same percentage estimated for normalized σ_y. Again, the impact of the nanofiber's stiffness play opposite role on the escalading Von Misses stresses which have range of 58.4 to 64.3 % as $E_f = 400$ to 1000 GPa respectively.

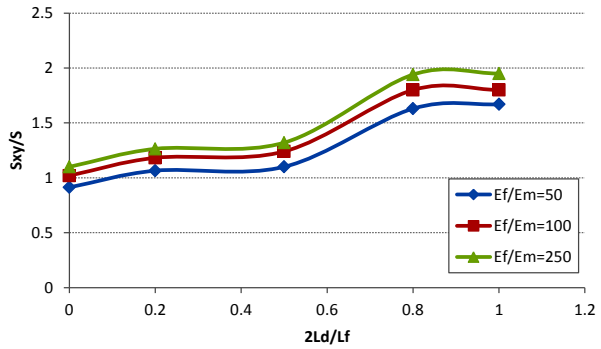

Fig. 6 – Normalized Von Misses stress of transverse side σ_{Von} / σ versus total debonding length over nanofiber's length

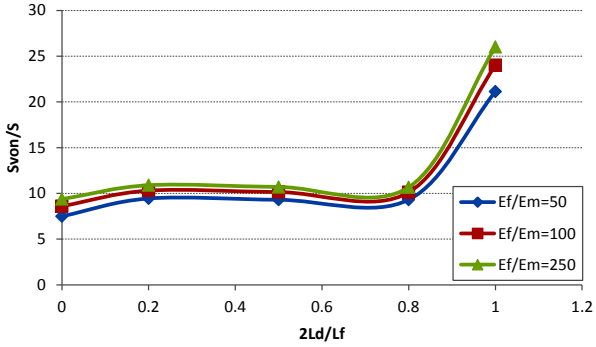

Fig. 7 – Normalized Von Misses of longitudinal side σ_{Von} / σ versus total debonding length over nanofiber's length

The third stage of the analysis is to investigate the shear σ_{xy} and the Von Misses stresses on the longitudinal side of the nanofiber. Figure 5 shows that as the debonding increases, a slight increase in normalized shear stresses is observed, which starts from 16.6 % at $2L_d / L_f = 0.2$, and remains almost stable until the debonding approaches 50 % of the nanofiber's length, so it starts to increase to 78.5 % at $L_d = 80$ nm and becomes quit steady as RVE being fully debonded. This is for the case where $E_f / E_m = 50$. A similar behavior for the other ration, i.e., $E_f / E_m = 100$ and 250, but with greater level of stresses. The maximum growth in normalized shear stresses can be as 76.4 to 77 % for the $E_f = 400$ and 1000 GPa respectively.

On the contrary, Von Misses stresses on the longitudinal side of the nanofiber don't show similar behavior as in the transverse side. The stresses show increase of 25.9 % as $L_d = 10$ nm, and remains stable between $2L_d / L_f = 0.2$ to 0.8, and then large jump in Von Misses stresses approaches to 181.7 % as RVE becomes fully debonded. This analysis for $E_f / E_m = 50$, for the other values, the maximum stresses are 179 and 177.5 % whenever $E_f = 400$ and 1000 GPa respectively.

5. CONCLUSIONS

3D-axisymmetric finite element analysis was used to investigate cylindrical RVE with circumferential debonding. Mainly, the debonding has negative impact on the effective stiffness of the nanocomposite, and this is reflected on the increase in the normal stresses on the transverse side as well as the shear stresses along the longitudinal side of the nanofiber of the RVE. Whereas Von Misses stresses on the both sides of the nanofiber were increased in different levels. The influence of the nanofiber's stiffness has less impact than expected. Eventually, whatever debonding initiation cause, still is considered as one of the major factors that lead to the final failure of the nanocomposite due to increasing in the level of the stresses as losing interfacial contact areas which through stresses transfer.

REFERENCES

1. L.R. Xu, S. Sengupta, *J. Nanosci. Nanotechnol.* **10**, 1 (2005).
2. P.M. Ajayan, L.S. Schadler, P.V. Braun, *Nanocompsite Science and Technology* (Wiley-VCH Verlag GmbH Co. K GaA, Weinheim, 2003).
3. H.D. Wagner, O. Lourie, Y. Feldman, R. Tenne, *Appl. Phys. Lett.* **72**, 188 (1998).
4. J. Njuguna, K. Pielichowski, *Adv. Eng. Mater.* **6**, 204 (2004).
5. M.F. Yu, O. Lourie, M. Dyer, K. Moloni, T. Kelly, R.S. Ruoff, *Science* **287**, 637 (2000).
6. L.S. Schadler, S.C. Giannaris, P.M. Ajayan, *Appl. Phys. Lett.* **73**, 3842 (1998).
7. M. Bourchak, B. Kada, M. Alharbi, K. Aljuhany, *Int. J. Nanopart.* **2**, 467 (2009).
8. L.R. Xu, V. Bhamidipati, W. Zhong, J. Li, C.M. Lukehart, E. Lara-Curzio, K.C. Liu, M.J. Lance, *J. Comp. Mat.* **38**, 1563 (2004).
9. L.R. Xu, S., *J. Nanosci. Nanotechnol.* **5**, 620 (2005).
10. K.T. Lau, S.Q. Shi, L.M. Zhou, H.M. Cheng, *J. Comp. Mat.* **37**, 365 (2003).
11. D. Srivastava, C. Wei, K. Cho, *ASME Appl. Mech. Rev.* **56**, 215 (2003).
12. W.K. Ahmed, K. Aslantas, Y. Al-Doury, *J. Nanostruct. Polym. Nanocompos.* **9** No 3 (2013).
13. W.K. Ahmed, S.A. Shakir, *The Int. J. Nanoelectron. Mater.* Accepted 23 April 2013. [In press].
14. W.K. Ahmed, W.N. Al Rifaie, *Phys. Rev. Res. Int.* **3** No 4, 438 (2013).
15. A.A. Gawandi, J.M. Whitney, G.P. Tandon, R.B. Brockman, *Compos. Part B: Eng.* **40**, 698 (2009).
16. K. Yazdchi, M. Salehi, *Compos. Part A: Appl. S.* **42**, 1301 (2011).
17. L.H. Shao, R.Y. Luo, S.L. Bai, J. Wang, *Compos. Struct.* **87**, 274 (2009).
18. R.D. Peng, H.W. Zhou, H.W. Wang, L. Mishnaevsky Jr., *Comp. Mat. Sci.* **60**, 19 (2012).
19. Y.J. Liu, N. Xu, *Mech. Mat.* **32**, 769 (2000).
20. D. Luo, W. Wang, Y. Takao, *Comp. Sci. Technol.* **67**, 2947 (2007).
21. H. Hua, L. Onyebuekea, A. Abatanb, *J. Miner. Mat. Charact. Eng.* **9**, 275 (2010).
22. U.A. Joshi, S.C. Sharma, S.P. Harsha, *Comp. Mat. Sci.* **50**, 3245 (2011).
23. K.P. Saffar, N.J. Pour, A.R. Najafi, G. Rouhi, A.R. Arshi, A. Fereidoon, *World Academy Sci., Eng. Tech.* **23** (2008).
24. X.L. Chen, Y.J. Liu, *Comp. Mat. Sci.* **29**, 1 (2004).
25. R. Rafiee, A. Fereidoon, M. Heidarhaei, *Comp. Mat. Sci.* **56**, 25 (2012).
26. M.M. Shokrieh, R. Rafiee, *Comp. Struct.* **92**, 647 (2010).
27. X. Lu, Z. Hu, *Compos. Part B: Eng.* **43**, 1902 (2012).
28. K.I. Tserpes, A. Chanteli, *Comp. Struct.* **99**, 366 (2013).
29. P. Papanikos, D.D. Nikolopoulos, K.I. Tserpes, *Comp. Mat. Sci.* **43**, 345 (2008).
30. M. Meo, M. Rossi, *Mat. Sci. Eng. A* **454-455**, 170 (2007).
31. A. Hernández-Pérez, F. Avilés, *Comp. Mat. Sci.* **47**, 926 (2010).
32. M. Meo, M. Rossi, *Comp. Sci. Technol.* **66**, 1597 (2006).